Electro-chemical Corrosion of a Cast Iron Protected with a Al_2O_3 Ceramic Layer

COSTICA BEJINARIU[1], CORNELIU MUNTEANU[1], COSTEL DOREL FLOREA[1], BOGDAN ISTRATE[1], NICANOR CIMPOESU[1]*, ADRIAN ALEXANDRU[1], ANDREI VICTOR SANDU[1,2]*

[1]Gheorghe Asachi Technical University of Iasi, Faculty of Materials Science and Engineering, 67 D. Mangeron Str., 700050, Iasi, Romania

[2] Romanian Inventors Forum, 3 Sf. P. Movila Str., 700089, Iasi, Romania

Thin layers of Al_2O_3 were used to protect a standard FC250 cast iron at electro-corrosion in acid rain electrolyte solution. In comparison with a cast-iron material we present the results obtained on the metallic covered sample using linear and cyclic potentiometry. The material surface was investigated using scanning electron microscopy (SEM) and energy dispersive spectroscopy (EDS) techniques. The results present a generalized corrosion with a higher resistance for covered samples (more than 30 times) in comparison with the simple cast iron. The main causes of the corrosion of the covered samples are based on the thin ceramic layer imperfections like pores or micro-cracks that facilitate the contact of the electrolyte solution with the metallic substrate.

Keywords: ceramic layer, electro-corrosion, cast iron, potentiometry, SEM-EDX

.

The research and characterization of materials used to build vehicle brake discs is an area of high interest for a wide range of applications and demand from the automotive market [1, 2]. According to the International Organization of Motor Vehicle Manufacturers (OICA), approximately 60 million cars are produced annually over the last three years, and the threshold of 50 million was first passed in 2007. Romania ranks 26th in the world with the number of cars produced annually (about 320,000 cars around 0.5% of total production), ranking by China, Japan and Germany (24%, 11.9% and 10% respectively total of machines). Now it is estimated that there are more than 1.5 billion cars on the streets. During the operation of these vehicles, at least one billion braking systems operate constantly and wear the brake discs until they are replaced [3, 4]. At the moment, they all use braking systems with more than 99% brake disks made of metallic materials [5]. The most commonly used materials in this field are cast iron that has good anti-friction properties and a low production price [6-8]. As new trend, but expensive, is the usage of ceramic materials to obtain breaking disks. At this moment only few applications of 3D printed ceramic materials are used for special fields like Grand Prix tournament mono-posts [9].

Deposition method based on plasma spraying in atmosphere, vacuum or inert gas use gas flows at a high temperature in order to melt the powders of the material proposed for thin layer formation [10]. The powders are heated in electric arc until the deposition material reach plasma state and form a high heated flux orientated toward the substrate target. In plasma spraying deposition process the temperatures, depending on the nature of the powders, usually pass the 16000 K value [11-13]. At industrial and laboratory level the plasma deposition technique can be appreciate one of the most used method of all thermal spray deposition. At present, there are industrial branches where the use of thermal heaters is indispensable in order to obtain the characteristics required by the beneficiaries. Among the most advanced areas, in the case of the use of components of covered materials, the aerospace and automotive industries are particularly reminded [12-14].

In this paper we follow the influence of a ceramic layer (Al_2O_3) on the electro-chemical resistance of a cast iron material (FC250) deposited through plasma spraying.

Experimental part

In order to increase the corrosion and wear resistance of standard FC cast iron material, used for automotive industry at breaking system, using ceramic thin layers. The equipment used to obtain the ceramic layers was SULZER METCO 9MCE an air plasma deposition system with industrial applications [15, 16]. In table 1 are presented the technological parameters used for coating process. The dimensional details of the equipment and the sample holder are presented in figure 1.

Table 1
TECHNOLOGICAL PARAMETERS USED FOR COATING PROCESS

Powder	Gun	Ar		H_2		Electric		Powder feeder 9MP			Spray distance (inch)
		Pressure (psig)	Gas flow (SCFH)	Pressure (psig)	Gas flow (SCFH)	DC (A)	DC (V)	Carrier gas flow (SCFH)	Air Preasure (psig)	Rate (lb/h)	
Al_2O_3	9MB	75	111	50	10	500	60-70	13.5	20	5.5	3.5

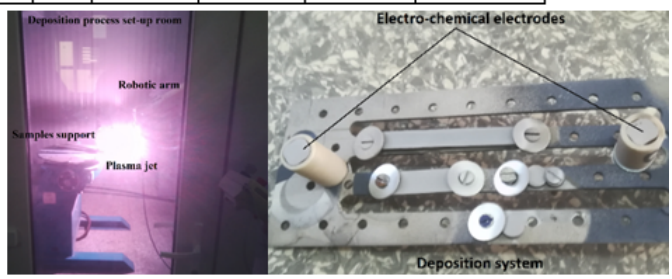

Fig.1. Experimental set-up for ceramic layers' deposition with a detail of the samples support

* email:nicanornick@yahoo.com; andrew_viktor@yahoo.com

For microstructural, chemical composition and electro-chemical experiments different samples were prepared for deposition of ceramic layers using plasma deposition method. For microstructural and chemical composition cylindrical samples (10 mm diameter and 3 mm thickness) and for electro-chemical tests samples with diameter of 10 mm were isolated in Teflon material. The experimental set-up for deposition is presented in figure 1.

The experiments consist of two deposition conditions:

-Two passing times with plasma flow (around 12 µm per pas [15] obtaining a 25µm ceramic layer on the metallic surface);

-Four passing times with plasma flow (around 12 µm per pas [15] obtaining a 50 µm ceramic layer on the metallic surface).

Before the deposition process all the samples surface was prepared by grinding with sandblast in order to improve the adherence of the ceramic layer to the metallic substrate [17]. For deposition process the equipment can cover big surfaces until 4 m^2 in a very short time representing a proper solution for industrial applications. A rotated support table helps the deposition process to be faster for different experimental substrate (different alloys, shape or dimensions).

After the electrochemical experiments (linear and cyclic potentiometry on potentiostat equipment (PGP 201) with a three electrodes cell was used for tests) the material was cleaned by sonication for 60 min in technical alcohol [18-20]. The electrolyte solution used for experiments was acid rain. Sulfuric acid (H_2SO_4), nitric acid (HNO_3), and carbonic acid (H_2CO_3) are the major components of acid rain. These chemicals are released into the atmosphere naturally however prior to industrialization and the advent of factories and reliance on hydrocarbons (coal, gasoline, crude oil, et cetera) acid rain was a rare event. In recent decades' acid rain has become an increasingly common event especially in highly industrialized areas and highly agglomerate auto cities.

The experimental samples surface was analyzed using SEM equipment (scanning electron microscopy with VegaTescan LMH II, VegaT software for 2D characterization) and EDAX detector (X-ray energy dispersive spectroscopy, Bruker type, Esprit software) for structural and chemical analyses [21-26].

Results and discussions

Experimental results present the electro-corrosion resistance of three samples (substrate cast iron FC250, FC250 + 2 layers of Al_2O_3 ceramic material ~25 µm and FC250 + 4 layers of Al_2O_3 ceramic material ~50 µm) in acid rain electrolyte solution. In figure 2 are presented the potentio-dynamic linear polarization curves of Al_2O_3 coating layers of different thicknesses on FC250 cast iron in comparison with free FC250 substrate and in figure 2b the cyclic polarization curves. The linear polarization curves were plotted within the potential range: 0.8 and 1.0 V using a scanning speed of 1 mV/s [27]. The corrosion rate may correlate with the intensity of the corrosion current or the current density based on Faraday's law [28]. For the experimental cases corrosion rates were obtained in the order of millimeters per year for FC250 material and micrometers for covered metallic materials. From figure 2a can be observed a big difference between the behavior of the cast iron material and the cast iron with ceramic layers. The difference is not that evident for cyclic polarization curves (fig. 2b). The covered samples present a similar behavior both with an almost inexistent anodic reaction.

The cathodic curve of the cyclic curves (fig. 2b), present a similar path as the anodic curve -having a reduce hysteresis, and the current densities in the passive region are similar to those recorded during direct (anodic) scanning at the same potential [29]. Small difference between the anodic and cathodic line (meaning the miss of a loop) is connected to the stability of the surface and the competition between diffusion and dissolution in case of localized corrosion points. Pitting corrosion appears based on a very fast process of diffusion with semi-circle dimensional aspect. In the first part of the cathodic part (reversing line) the effects of dissolution process are reduced and the time for continue the diffusion is limited and usually not enough.

The main parameters of the corrosion process (E_0 and j_{cor}) obtained by processing the linear polarization curves are centralized in table 2. The corrosion current thus determined is in fact the corrosion current occurring at the metal/corrosive environment interface when the metal is immersed in the solution and cannot be measured directly by electrochemical methods.

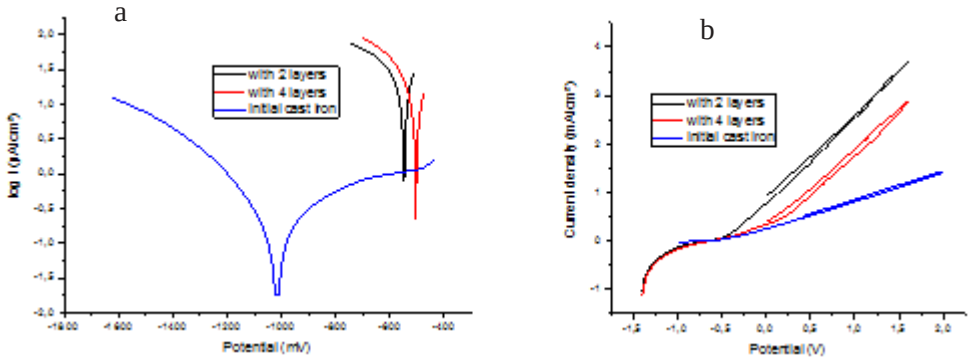

Fig. 2. a) Potentio-dynamic linear polarization curves of Al_2O_3 coating layers of different thicknesses on FC250 cast iron in comparison with free FC250 substrate and b) cyclic polarization curves.

Table 2

ELECTRO-CHEMICAL PARAMETERS AFTER THE ELECTRO-CORROSION TESTS IN ACID RAIN ELECTROLYTE SOLUTION

Sample	OCP mV	E_0 mV	b_a mV	b_c mV	R_p ohm.cm²	J_{cor} µA/cm²	V_{cor} mm/year
Cast iron+2 ceramic layers	-491	548.7	-	-469.5	1450	29.8112	0.12
Cast iron+4 ceramic layers	-430	504.6	-	-338.0	1970	25.7842	0.10
Initial cast iron	-716	-1017.0	660.4	-348.3	323.57	137.7	3.645

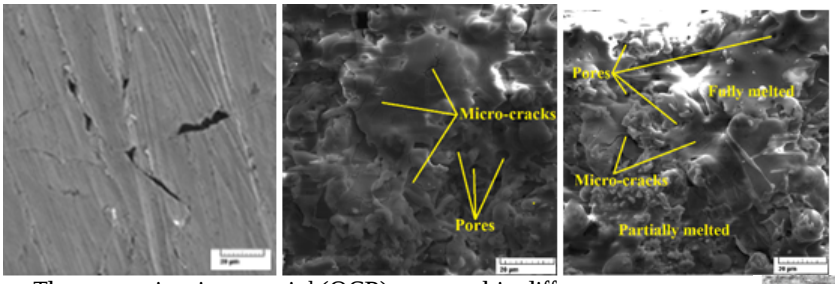

Fig. 3. SEM images of a) cast iron FC250, b) FC250 + 2 layers of ceramic material and c) FC250 + 4 layers of ceramic material.

The open circuit potential (OCP) present big differences between the FC250 material and FC250 + ceramic layer based on the influence of the inert material layer on the corrosion resistance. The polarization resistance approved the OCP values and strictly in accordance with the corrosion current. The corrosion current of the initial material (FC250) is 4 to 5 times bigger in comparison with the value registered for the samples with ceramic layer. The corrosion rate is 30 to 40 times bigger in the FC250 material case in comparison with the covered samples.

Scanning electron microscopy (SEM) (VegaTescan LMH II) was applied to analyze the coating morphology also the structure of FC250 material (fig. 3).

In figure 3b and c), the micrograph of the coating displays a dense microstructure with high cohesion and small surface cracks. Moreover, figure 3 displays a few porous areas in both coated samples. Based on the deposition process cracks and pores form vertically into splats. The main cause for the appearance of these defects is the time of rapid solidification of the material in atmosphere and the temperature difference between the layers.

The surface of the layer in first deposition case, with two layers, present fully melted area of the material in comparison with the sample with four layers deposited were partially melted areas present not-melted part of powder. A relative degree of homogeneity of the coating layer is crucial for increase of the corrosion resistance of the substrate [25].

In figure 4 are presented the SEM images of the experimental materials surface after the electro-chemical tests: cast iron FC250 (fig. 4a and b), FC250 + 2 layers (fig. 4c and d), FC250 + 4 layers (fig. 4e and f), at two different amplification scales.

In all cases, figure 4, is confirmed the generalized corrosion observed from cyclic curves (fig. 2b), without specific corrosion areas (pitting corrosion). Parts of the coatings (fig. 4d and f) present, in particular areas represented by ceramic material particles, a pitting corrosion type at the exterior part of the layer. If the environment continues to be aggressive (the dissolving rate is high enough to exceed the diffusion) the pitting points appeared at the surface of the ceramic layer may penetrate the ceramic layer. In the covered samples case also an aggressive surface attack is observed even the resistance of the exterior oxide layer sustain a high resistance. Normally the inert behavior of the ceramic materials (like alumina) should keep intact the metallic surface protecting the substrate material. The pores and micro-cracks in

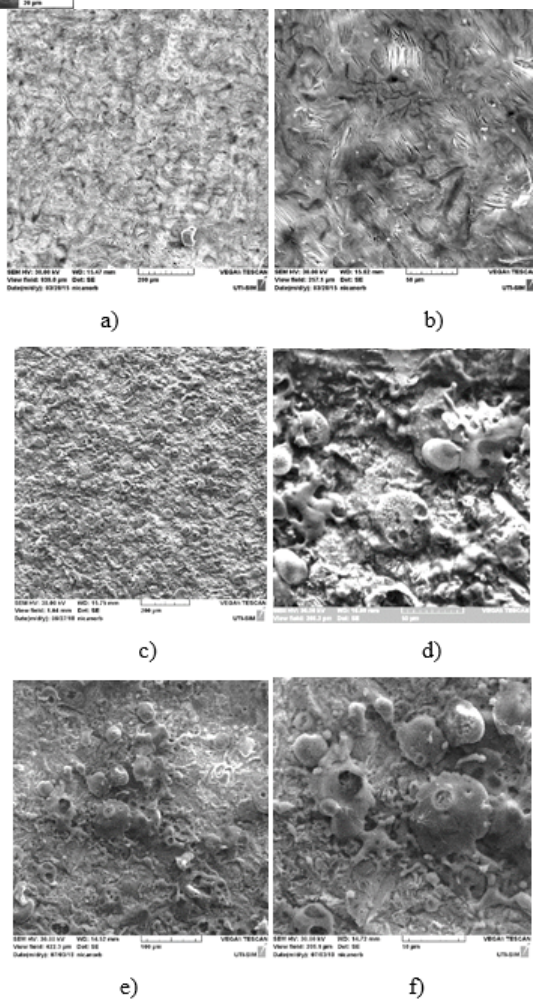

Fig. 4. SEM images of surface after the electro-chemical tests a) and b) cast iron FC250, c) and d) FC250 + 2 layers and e) and f) FC250 + 4 layers

coatings became relatively more and bigger because the original micro pores were damaged. The main cause of the corrosion is given by the initial existence of the pores and cracks in the initial state of the coatings. The higher magnification SEM micrographs, as presented in figure 4d and f suggested that the corrosion damage was confined mostly to the coating defects (i.e. pores and cracks). It can be seen that some prolate spheroid corrosion products were formed at the coating defects.

The EDS analysis results (table 3) revealed that the corrosion products were mainly composed of Fe and O. It

Table 3

CHEMICAL COMPOSITION OF THE EXPERIMENTAL MATERIALS AFTER THE ELECTRO-CORROSION RESISTANCE TEST

Element/ sample	Fe		O		Al		C		Si	
	wt%	at%	wt%	at%	wt%	at%	wt%	at%	wt%	at%
FC250	50.56	22.39	42.13	65.13	-	-	3.4	6.9	3.9	3.7
FC250+2 layers	32.03	14.7	37.16	49.52	23.93	18.75	4.53	10.85	2.33	1.78
FC250+4 layers	33.89	16.77	30.67	45.73	26.93	27.58	4.86	11.12	3.3	3.2
Error EDS	0.7		0.95		0.5		0.8		0.1	

proved that electrochemical corrosion generally occurred on the cast iron substrate during electro-chemical experiments.

The corrosion process occurs mainly through cracks and pores from the ceramic layer which allows the contact of the electrolyte solution with the metallic substrate. In all three cases the materials present an accentuated oxidation of the surface, especially on the FC250 material because a part of the oxygen in the other cases most of the oxygen is of the coating layer and only a percentage participate in oxides formation. Generally, especially were the ceramic layer was penetrated till the substrate, on the surface appear iron oxides. Since the ceramic top coat and the metallic bond coat were all very passive there was no big difference on the electric potentials of them.

Conclusions

Coatings of Al_2O_3 were made on a cast iron material by atmospheric plasma spraying. The electro-corrosion behavior of these coatings (25 respectively 50 µm thickness) was analyzed using electro-chemical methods (linear and cyclic polarization), complemented by SEM and EDX. The main conclusions are:

-both atmospheric plasma sprayed Al_2O_3 present micro-pores, laminar splats and straight columnar grains;

-in comparison with the initial material (un-covered FC250) both materials with ceramic layers present a superior electro-corrosion resistance with values of 30 to 40 times bigger;

-the defects in Al_2O_3 thinner layer (25 µm) coating were relatively few compared to the thicker coating, and hence, the corrosion resistance of the was a little better;

-it can be appreciating that the porosity and the presence of micro-cracks and pores had direct effect on the corrosion resistance and rate of the plasma sprayed coatings.

References

1. SUGISHITA, J., FUJIYOSHI, S., Wear, **66**, 1981, p. 209.
2. TKAYA, M.B., MEZLINI, S., MANSORI, M.E., ZAHOUANI, H., Wear, **267**, 2009, p. 535.
3. BLAU, P.J., MEYER, H.M., Wear, 255, 2003, p. 1261.
4. PRASAD, B.K., Materials Science and Engineering A, **456**, 2007, p. 373.
5. ELBEL, T., SENBERGER, J., ZADERA, A., HAMPL, J., Archives of Materials Science and Engineering, **33**, 2008, p. 111.
6. CAMPBELL, J., Metallurgical and Materials Transactions B, **40**, 2009, p. 786.
7. NADEL, J., EYRE, T.S., Tribology International, **11**, no. 5, 1978, p. 267.
8. TOMLINSON, W.J., DENNISON, G., Tribology International, **22**, 1989, p. 259.
9. ZAVAREH, M.A., DOUSTMOHAMMADI, E., SARHAN, A.A.D.M., KARIMZADEH, R., NIA, P.M., SINGH, R.S.A.K., Ceram. Int., **44**, no. 11, 2018, p. 12180.
10. BABU, P.S., SEN, D., JYOTHIRMAYI, A., KRISHNA, L.R., RAO, D.S., Ceram. Int., **44**, no. 2, 2018, p. 2351.
11. LIU, Z., DONG, Y., CHU, Z., YANG, Y., LI, Y., YAN, D., Mater. Des., **52**, 2013, p. 630.
12. SANDU, A.V., CODDET, C., BEJINARIU, C., J. Optoelectron. Adv. Mater. **14**, 2012, p. 699.
13. ZHANG, C., YANG, Y., MIAO, L., MA, Y., ZHANG, X., CUI, Y. DONG, Y., CHEN, X., WANG, L., LIU, Z., Surf. Coat. Technol. **350**, 2018, p. 550.
14. LIU, Z., CHU, Z., DONG, Y., YANG, Y., CHEN, X., KONG, X., YAN, D., Vacuum, **101**, 2014, p. 6.
15. FLOREA, C., BEJINARIU, C., MUNTEANU, C., CIMPOESU, N., Preliminary Results on Complex Ceramic Layers Deposition by Atmospheric Plasma Spraying, Advanced Materials Engineering and Technology V, Amer. Inst. Physics: Melville, Vol. 1835, 2017. p. UNSP 020053 ISBN 978-0-7354-1505-8.
16. COSERI, S., SPATAREANU, A., SACARESCU, L., SOCOLIUC, V., STRATULAT, I.S., HARABAGIU, V., J. Appl. Polym. Sci., **133**, no. 5, 2016, 42926.
17. FLOREA, C.D., MUNTEANU, C., CIMPOESU, N., SANDU, I.G., BACIU, C., BEJINARIU, C., Rev. Chim. (Bucharest), **68**, no. 11, 2017, p. 2582.
18. FLOREA, C.D., CARCEA, I., CIMPOESU, R., TOMA, S.L., SANDU, I.G., BEJINARIU, C., Rev. Chim.(Bucharest), **68**, no. 10, 2017, p. 2397.
19. GRADINARU, I., BACIU, R.-E., CIMPOESU, R., TOMA, D., BACIU, M., Rom. J. Oral Rehabil., **9**, 2017, p. 73.
20. ZAHARIA, M.G., STANCIU, S., CIMPOESU, R., IONITA, I., CIMPOESU, N., Appl. Surf. Sci., **438**, 2018, p. 20.
21. BACIU, C., BACIU, E.R., CIMPOESU, R., LEVENTE, C.G., BOSINCEANU, D.G., BACIU, M., BEJINARIU, C., Microstructural Analysis of Ti-Based Shape Memory Alloys Following the Electrochemical Corrosion in Artificial Saliva, International Conference on Innovative Research - ICIR Euroinvent 2017; SANDU, A.V., ABDULLAH, M.M.A., VIZUREANU, P., GHAZALI, C.M.R., SANDU, I., Eds.; IOP Publishing Ltd: Bristol, **209**, 2017, p. 12033.
22. STIRBU, I., VIZUREANU, P., CIMPOESU, R., DASCALU, G., GURLUI, S.O., BERNEVIG, M, BENCHEA, M., CIMPOESU, N., POSTOLACHE, P., Journal of Optoelectronics and Advanced Materials, **17**, no. 7-9, 2015, p. 1179.
23. STRAT, M., VASILIU, S., STRAT, G., LUCA, C., GRECU, I., GURLUI, S., STRATULAT, S.I., J. Optoelectron. Adv. Mater., **8**, no. 1, 2006, p. 181.
24. VITALARIU, A., LEATA, R., CHELARIU, R., MUNTEANU, C., CIMPOESU, R., ILIE, M., COMANECI, R., MOISEI, M., Rev. Chim.(Bucharest), **66**, 2015, p. 2147.
25. NEDEFF, V., BEJENARIU, C., LAZAR, G., AGOP, M., Powder Technol., **235**, 2013, p. 685.
26. NICA, P.-E., AGOP, M., GURLUI, S., BEJINARIU, C., FOCSA, C., Jpn. J. Appl. Phys., **51**, 2012, No Paper: 106102.
27. CIMPOESU, N., TRINCA, L.C., DASCALU, G., STANCIU, S., GURLUI, S.O., MARECI, D., J. Chem., **2016**, 2016, No Paper: 9520972.
28. IZQUIERDO, J., BOLAT, G., CIMPOESU, N., TRINCA, L.C., MARECI, D., SOUTO, R.M., Appl. Surf. Sci., **385**, 2016, p. 368.
29. CIMPOESU, N., SANDULACHE, F., ISTRATE, B., CIMPOESU, R., ZEGAN, G., Metals, **8**, 2018, p. 541.

Manuscript received: 14.08.2018